ACS APPLIED MATERIALS & INTERFACES

www.acsami.org

Research Article

# Probing the Critical Role of Interfaces for Superior Performance in PbS Quantum Dot/Graphene Nanohybrid Broadband Photodetectors

Andrew Shultz,* Bo Liu, Maogang Gong, Hugo Barragan Vargas, Francisco C. Robles Hernandez, and Judy Z. Wu*

Cite This: *ACS Appl. Mater. Interfaces* 2024, 16, 21302−21310

Read Online

ACCESS | Metrics & More | Article Recommendations | Supporting Information

**ABSTRACT:** Colloidal quantum dots/graphene (QD/Gr) nanohybrids have been studied intensively for photodetection in a broadband spectrum including ultraviolet, visible, near-infrared, and shortwave infrared (UV−vis-NIR-SWIR). Since the optoelectronic process in the QD/Gr nanohybrid relies on the photogenerated charge carrier transfer from QDs to graphene, understanding the role of the QD−QD and QD−Gr interfaces is imperative to the QD/Gr nanohybrid photodetection. Herein, a systematic study is carried out to probe the effect of these interfaces on the noise, photoresponse, and specific detectivity in the UV−vis-NIR-SWIR spectrum. Interestingly, the photoresponse has been found to be negligible without a 3-mercaptopropionic acid (MPA) ligand exchange, moderate with a single ligand exchange after all QD layers are deposited on graphene, and maximum if it is performed after each QD layer deposition up to five layers of total QD thickness of 260−280 nm. Furthermore, exposure of graphene to C-band UV (UVC) for a short period of 4−5 min before QD deposition leads to improved photoresponse via removal of polar molecules at the QD/Gr interface. With the combination of the MPA ligand exchange and UVC exposure, optimal optoelectronic properties can be obtained on the PbS QD/Gr nanohybrids with high specific detectivity up to $2.6 \times 10^{11}$, $1.5 \times 10^{11}$, $5 \times 10^{10}$, and $1.9 \times 10^{9}$ Jones at 400, 550, 1000, and 1700 nm, respectively, making the nanohybrids promising for broadband photodetection.

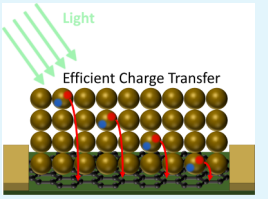


**KEYWORDS:** *interface, photodetector, quantum dots, nanohybrid, broadband*



## 1. INTRODUCTION

The colloidal quantum dots (QDs)/graphene (Gr) nanohybrid heterostructure (QD/Gr) takes advantage of the strong quantum confinement in both materials that results from the low dimensionality of each.[1] In graphene, this confinement leads to exceptional charge carrier mobility at room temperature.[2−7] On the other hand, quantum confinement in QDs leads to benefits in the form of enhanced light-matter interaction, spectral tunability, suppressed phonon scattering, and multiple exciton generation.[8−14] For example, PbS QDs have a broadband absorption covering from ultraviolet to visible that could be further extended to near-infrared (NIR) and shortwave-infrared (SWIR) via QD size tuning. Recently, specific detectivities ($D^*$) of $10^{13}$ and $10^{12}$ Jones have been reported under 532 nm (visible) and 1550 nm (SWIR) incident wavelength, respectively, on PbS QD/Gr nanohybrid photodetectors.[1] In fact, interest in nanohybrids comprised of many different materials (such as $WS_2$, $WSe_2$, $MoS_2$, ZnO, graphite, $Bi_2Se_3$, and $CsPbBr_2I$ to name a few) has been increasing for over a decade as the expected next generation of photodetectors and solar cells with the promise to be made into flexible devices.[15−25]

In the QD/Gr nanohybrid photodetectors, the optoelectronic process includes three steps: light absorption by the QD film typically consisting of multilayers of QDs of a few nanometers in diameter, dissociation of photogenerated excitons (electron−hole pairs) in the QDs, and charge transfer from QD film to graphene driven by the built-in electric field due to the band-edge alignment at the QD/Gr interface. It should be noted that after one type of charge carriers is transferred to graphene the other oppositely charged carrier is trapped in the QDs before charge recombination occurs.[26] The consequent photogating effect on graphene results in the electrical conductivity change of the graphene channel as the photoresponse. Therefore, the optoelectronic process is affected sensitively by two major kinds of interfaces: the QD−QD interface and the QD-Gr interface, since the photogenerated charge carriers must travel through multiple QD−QD interfaces in the QD film of multiple QD layers and across the QD−Gr interface to complete the optoelectronic process. In probing the PbS QD/Gr nanohybrid at different temperatures, Grotevent et al. reported an order of magnitude lower $D^*$ at 1280 nm measured at room temperature

Received: January 19, 2024
Revised: March 19, 2024
Accepted: March 28, 2024
Published: April 9, 2024

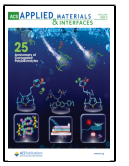




https://doi.org/10.1021/acsami.4c01115
*ACS Appl. Mater. Interfaces* 2024, 16, 21302−21310

compared to the same measurement at 80 K, suggesting the performance limiting factors may affect the PbS QD/Gr interface more at higher temperatures.[27] A hypothesis is that the defects and adsorbed molecules on the surface of QDs and graphene may have a critical impact on the charge transfer at the interfaces of the QD/Gr nanohybrids at room temperature, while this impact could be reduced significantly at lower temperatures when the motion and functionality of the defects and molecules are suppressed. Since uncooled photodetectors are preferred for a large spectrum of applications, understanding role of the interfaces through which to control the QD/Gr interface is essential to optimization of uncooled QD/Gr photodetector performance.[27]

Motivated by this, the PbS QD/Gr nanohybrid was selected in this work to probe the role of interfaces on the noise and photoresponse in the broadband spectrum of ultraviolet, visible, NIR, and SWIR (UV−vis-NIR-SWIR in 400−1700 nm wavelength range) at room temperature. We found that charge transfer may be blocked if molecules from the QD synthesis solvents and from air are present at the PbS QD-QD and QD/Gr interfaces. In order to address this issue, we have developed interface engineering processes, including C-band UV light (UVC) irradiation of graphene before QD deposition and ligand exchange (LE) after each QD layer deposition. UVC irradiation removes insulating residues that block charge transfer to graphene as well as the polar molecules that trap charge at the QD−Gr interface, resulting in an increased photoresponse and faster response speed. Interestingly, we have found that these polar molecules can be temporarily removed from graphene with a moderate irradiation by UVC, allowing PbS QD deposition to be completed before they reattach to graphene. Additionally, LE is performed after deposition of each PbS QD layer to link QD−QD and QD−Gr interfaces with stable and conductive ligands to facilitate charge transfer. With the combined layer-by-layer LE and UVC for optimal interfaces, a high photoresponse in the broadband of UV−vis-NIR-SWIR can be obtained.

## 2. EXPERIMENTAL SECTION

**a. Fabrication of QD/Gr Nanohybrid Devices.** Fabrication of the QD/Gr nanohybrid devices begins with cleaning the $SiO_2$/Si substrates using 3 rinsing cycles of acetone, isopropyl alcohol, and reverse osmosis water. Electrodes were patterned onto the substrate via a shadow mask and deposited using DC sputtering in a high vacuum chamber ($2.5 \times 10^{-7}$ Torr). The deposited electrodes are 40 nm Nb followed by 10 nm of Pd. The working gas was Ar at a pressure of 14 mTorr/30 mTorr with a sputtering power of 75 W/87 W for Nb/Pd, respectively. Each sample has four electrodes, each having dimensions of 4 mm (length) × 0.2 mm (width), allowing three devices to be obtained on each sample for consistency confirmation. Single layer graphene was grown on polycrystalline copper foil with a thickness of 50 $\mu$m (Sigma-Aldrich) using low pressure chemical vapor deposition at 1050 °C with $H_2/CH_4$ gases following our previously reported method.[28] The graphene was wet transferred onto the patterned electrodes using a wet transfer method reported on previously.[29,30]

PbS QDs were synthesized in an Ar environment using a Schlenk line system method and were suspended in hexane as we reported previously.[31] A Bioforce Nanosciences UV/Ozone ProCleaner was used prior to QD deposition for the specified samples. Deposition of the QDs was carried out by a micropipet to transfer 10 $\mu$L of suspended PbS QDs onto the substrate. A spin coater, operated at 3000 rpm for 1 min, was utilized to obtain a uniform thin film of PbS QDs. Efficient charge transfer from QDs to graphene as well as from QD to QD is necessary for high-performance devices.[26,32] In order to clean the graphene surface, UVC irradiation was employed on graphene before PbS QD deposition. The UVC irradiation was carried out in an Ozone Cleaner (ProCleaner plus) that has two emission wavelengths of 185 and 254 nm. The graphene/$SiO_2$/Si substrates were placed in the Ozone Cleaner and the UVC irradiation was carried out at room temperature of 22 °C for 4 min. It should be noted that UVC photons have fairly high energies of 4.9 eV (wavelength of 254 nm) and 6.7 eV (wavelength of 185 nm), which can induce desorption of residual molecules from the surface of the carbon nanostructures,[33,34] as well as effectively breaking the carbon−carbon bond on graphene.[35−37] A careful calibration of the UVC irradiation effect was carried out previously,[36,37] with the optimal condition of 4 min UVC treatment employed in this work. The insulating long-chain ligands of oleylamine (OLA) and oleic acid (OA) that encapsulate the QDs from the synthesis solvents must be exchanged with more conductive ones to facilitate charge transfer. Ligand exchange was performed by drop exposure of the QDs to 3-mercaptopropionic acid (MPA) to replace the OLA and OA ligands.[38] After coating PbS QDs on the substrate, 20 $\mu$L of MPA and methanol (1:1 mixture) were micropipetted on the sample followed by a 1 min wait duration with subsequent removal of the MPA/methanol mixture by spin coating for 1 min at 3000 rpm. Lastly, 20 $\mu$L of methanol was dropped on the sample to remove any residual MPA, this step was carried out twice. This deposition procedure was repeated a number of times to achieve multiple layers of PbS QDs. Finally, platinum wires that were soldered to the electrodes prior to QD deposition had the unconnected side soldered to a chip carrier that could be plugged into the readout electronics.

**b. Characterization of QD/Gr Nanohybrids.** Transmission electron microscopy (TEM) and high-resolution TEM (HRTEM) analysis of PbS QDs were carried out on a JEOL 2100 system with a field-emission filament and an accelerating voltage of 200 kV. For this study, the PbS QDs were deposited over a 300 mesh holey carbon Cu TEM grid. A UV-3600 Shimadzu spectrometer was used to measure the optical absorption spectra of the PbS QDs. Raman spectra, using a 488 nm excitation laser, were obtained for the graphene using a WiTec Alpha300 confocal micro-Raman system. The thickness of the PbS QD film was measured by using a KLA Tencor P-16 profiler. A Stanford Research Systems SR760 Fast Fourier Transform Spectrum Analyzer was employed to collect noise spectra for the fabricated samples.

**c. Optoelectronic Characterization of PbS QD/Gr Devices.** The spectral responsivity from 400 to 1000 nm was measured using a Newport Oriel Apex Monochromator Illuminator and a Newport Oriel Cornerstone 130 1/8m Monochromator. Diode lasers of output wavelengths of 1500 nm (SEI SLA5653) and 1700 nm (Eblana EP1735−0-DM-B06-FM) in the SWIR spectrum were used as the light source for optoelectronic characterization of the PbS QD/Gr nanohybrids. The power supply used with these diode lasers was an Arroyo Instruments 6310. Modulation of the light sources was achieved with a Thorlabs MC1000 optical chopper, and the resulting device photocurrent was measured using a CH Instruments 660D electrochemical workstation.

## 3. RESULTS AND DISCUSSION

Figure 1a exhibits schematically the device architecture of 2 electrodes connected by a graphene channel with PbS QDs deposited on top of the graphene channel. Each sample has four electrodes as shown in the upper-right inset of Figure 1a and hence consists of 3 devices to obtain reasonable statistics. The graphene channels are 0.2 mm long and 4 mm wide. The red arrows in the central graphic of Figure 1a indicate the two interfaces, QD-Gr (right) and QD-QD (left), whose charges must be transferred across to photogate the graphene after exciton dissociation. The built-in electric field at the QD-Gr interface is due to the band-edge alignment, as shown in the upper-left inset of Figure 1a, which drives the charge transfer from QDs to Gr. The graphene surface can be refined by UVC


https://doi.org/10.1021/acsami.4c01115
ACS Appl. Mater. Interfaces 2024, 16, 21302−21310

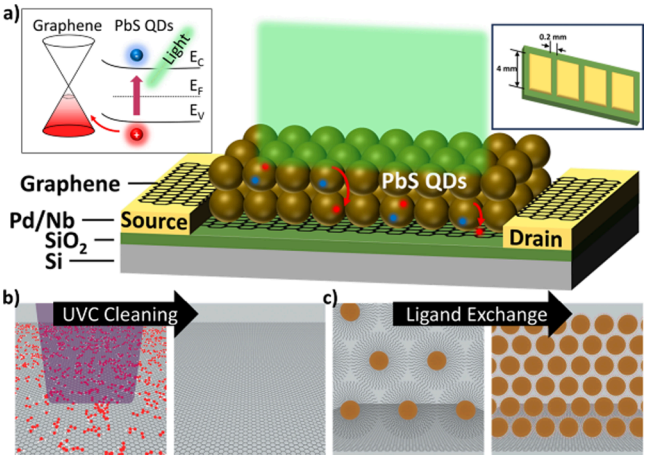


**Figure 1.** (a) Device design consists of 2 electrodes, a graphene channel, and photosensitive PbS QDs on top of the graphene. The upper-left inset depicts the interface energy band diagram between QD−Gr, while the upper-right inset shows the 3-device design adopted for this study. (b) Illustration showing the removal of polar molecules from graphene via UVC irradiation. (c) Exchange of long-chain insulating OLA and OA (left) with short-chain conducting MPA (right) ligands that surround the deposited QDs.

irradiation as depicted in Figure 1b to remove unwanted polar molecules and breakdown residual polymer left from the graphene transfer process. The second step to enhance the QD−QD and QD−Gr interface is the exchange of ligands surrounding the QDs from long-chain insulating OLA and OA to short-chain conductive MPA ligands, as shown schematically in Figure 1c.

Characterizations of the PbS QDs and graphene are shown in Figure 2. QD size and crystallinity were determined from the TEM data (Figure 2a). The HRTEM of a representative PbS QD in the inset of Figure 2a confirms the halite crystalline structure as expected for PbS with the lattice spacing of $d_{(220)}$ = 0.23 nm and $d_{(011)}$ = 0.41 nm, respectively. The HRTEM image in the inset of Figure 2b shows the presence of both Pb (black) and S (yellow) atoms, which is demonstrated by overlapping the simulated projections using Vesta software and the halite.cif file. The .cif file was obtained from the American Mineralogist Crystal Structure. Figure 2b shows the QDs size distribution with an average size of 8.4 nm. However, it is important to note that the QD size has a broad distribution in the range of 2−20 nm with ∼60% of the PbS QDs having sizes between 2 and 6 nm, as seen in Figure 2b.

The absorption spectrum of the PbS QDs can be seen in Figure 2c with an absorption peak at 1770 nm, and the broadband absorption is associated with the nonuniform size of the PbS QDs. Figure 2d contains a representative Raman spectrum for the graphene. Peaks at 1370 and 1610 $cm^{-1}$ are the so-called D and G bands corresponding to the in-plane vibrational mode and A1g breathing mode of the hexagonal rings, respectively. A third peak at 2740 $cm^{-1}$ is of the second order of the D band. Graphene quality can be determined from the height of the D band relative to the G band; a low D/G peak height ratio, as shown in Figure 2d, indicates a low concentration of defects in the graphene crystal structure. The number of graphene layers is typically determined from the 2D/G peak height ratio. Generally, a 2D/G ratio greater than 1.4 is considered monolayer.[28,39,40] 2D/G and D/G ratios of 2.57 and 0.14 were calculated from the spectrum shown in Figure 2d, confirming the graphene is a monolayer with negligible defects.

One of the interfaces scrutinized by this study is the QD−QD interface. At the heart of matter are capping ligands attached to the dangling bonds on the surface of the PbS QDs. Typically, OLA ligands are present after QD synthesis and are kept in place to help suspend the QDs for processing and protect the QDs from degradation that results when the uncapped surface is exposed to polar molecules.[41,42] However, the insulating OLA ligands hinder charge transfer from QDs to graphene, as shown in Figure 3a by the negligible photoresponse measured on a PbS QD/Gr device with OLA capped (red) PbS QDs. This means the insulating ligands must be replaced with conducting ligands, such as MPA, to enable charge transfer across QD−QD and QD−Gr interfaces. Indeed, a large photoresponse can be observed after LE with MPA (blue) on the same device, illustrating the critical effect of LE on the photoresponse (Figure 3a). A looming question exists of how complete the ligand exchange process is when comparing devices with a single layer of QDs versus multiple layers of QDs. Figure 3b compares 2 devices, one with a single QD deposition and the other with 6 depositions, both with a single LE step after the deposition(s). The negligible difference in the photocurrent between the two devices suggests that the additional 5 layers of PbS QDs make almost no contribution to the photoresponse. A possible explanation is that the majority of the OLA/OA capping ligands could not be exchanged with MPA effectively using the one-step LE after multiple QD layer depositions, as shown schematically in Figures 3c,d.

Prior to QD deposition, the graphene is cleaned by acetone and 2-propanol rinses to remove any residual PMMA left by the transfer as well as any dust or air particles that may have settled on the sample. Under the assumption that this may not be enough to guarantee a pristine graphene surface (for a clean QD-Gr interface), a UVC/ozone cleaner was utilized to provide further decontamination. The effects of the UVC treatment on noise current, photocurrent, and channel resistance are shown in Figure 4. Six samples were fabricated and exposed to 0, 2, 4, 5, 6, and 7 min of UVC. Before UVC irradiation, the resistance of each device on all samples was recorded. Immediately after the UVC radiation, the resistance and noise spectrum of each sample was measured followed by PbS QD deposition. There is little change in the noise spectrum of graphene as can be seen in Figures 4a,b. The error bars represent the standard deviation of the 3 devices on each sample. The dynamic response of an on/off cycle for illumination by a 1500 nm laser diode for a single device from each of the six samples is displayed in Figure 4c. From the dynamic photoresponse, it can be seen that the UVC treatment results in an enhanced photocurrent, the factor of enhancement being shown on the left-side *y*-axis of Figure 4d, for all irradiation durations. The maximum enhancement factor of 3.92 ± 0.55 was observed for a 4 min UVC exposure (green). Changes in resistance are shown on the right-side *y*-axis of Figure 4d, from which it can be seen that UVC durations greater than 4 min result in significant resistance increases. Raman spectra taken on a different set of samples (with only graphene) saw significant increases in the average D peak height for samples irradiated for longer than 4 min in UVC, indicating damage to the graphene (see Figure S2). Therefore, exposing graphene to moderate UVC irradiation prior to QD deposition likely improves the photoresponse by generating a cleaner QD-Gr interface. However, damage to


https://doi.org/10.1021/acsami.4c01115
ACS Appl. Mater. Interfaces 2024, 16, 21302−21310

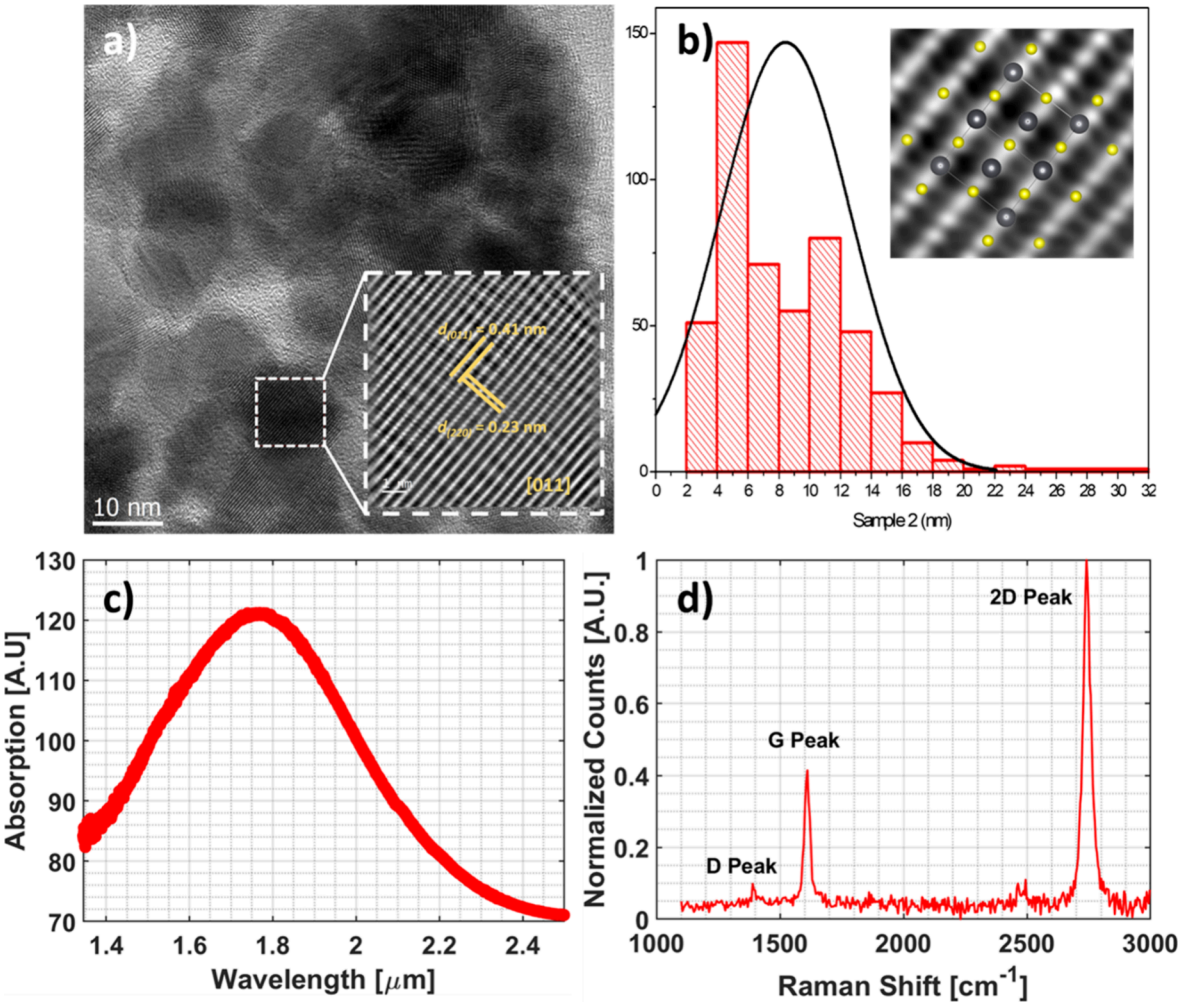


**Figure 2.** (a) TEM image of the PbS QDs showing the regular morphology of the PbS QDs. The inset exhibits the HRTEM image of a representative QD, which shows the location where the HRTEM FTT and IFTT were taken, respectively. (b) Histogram showing the PbS QD size distribution with an inset showing the Vesta projection of the PbS (halite) over the HRTEM image. (c) Absorption spectrum of the PbS QDs, and (d) Raman spectrum of the graphene.

graphene may occur for UVC exposure for longer than 4 min, which could reduce the benefits of the clean QD−Gr interface. Nevertheless, all five samples with UVC exposure times in the range of 2−7 min exhibit higher photoresponse than that of the unexposed counterpart (red), demonstrating the critical importance of a clean QD-Gr interface to charge transfer and hence optoelectronic performance of the QD/Gr nanohybrids.

With the understanding of the effect of UVC irradiation on the QD−Gr interface and LE on both Gr-QD and QD-QD interfaces, an additional question is raised of how thick the PbS QD film should be for maximum photoresponse if efficient charge transfer can be established across both QD−QD and QD−Gr interfaces. In order to answer this question, LE was performed after every PbS QD deposition up to six depositions on UVC treated graphene (4 min). Figure 5a shows that the QD thickness increases linearly with the number of QD depositions, as expected, with each deposition step increasing the QD film thickness by about 50 nm. The photoresponsivity ($R^*$) of a photodetector is defined as the ratio of the photocurrent to the illumination power upon the device,

$$R^* = \frac{I_L - I_D}{P_0} \quad (1)$$

Figure 5b displays the normalized $R^*$ measured at nine different wavelengths in the range of 400−1700 nm, at different stages in the device fabrication process, showing a drop in $R^*$ after every deposition step (D1 through D5) followed by an increase after every LE step (LE1 through LE5). Interestingly, a monotonic increase of $R^*$ with PbS QD depositions can be clearly seen in the broadband of UV−vis-NIR-SWIR. The normalization is made by dividing all $R^*$ values by that after the completion of LE5. This linear trend of the $R^*$ in Figure 5b suggests that the consecutive LE following each PbS QD deposition is effective in removing charge traps by the OLA/OA capping ligands and replacing them with conductive MPA ligands for optimal QD−QD and QD−Gr interfaces. The $R^*$ for 3 different devices on the sample as the function of increasing PbS QD film thickness is plotted in Figure 5c, indicating that QD layers higher than ∼250 nm (or five QD depositions) from the graphene do not contribute to the photoresponse (charges are either not collected or the photoinduced exciton in the QD is not dissociated). It should be noted that this thickness is comparable to that of the colloidal PbS QD heterojunction photodiode for maximal charge extraction and hence quantum efficiency.[43] The effect of the fabrication steps on the graphene noise is presented in


https://doi.org/10.1021/acsami.4c01115
ACS Appl. Mater. Interfaces 2024, 16, 21302−21310

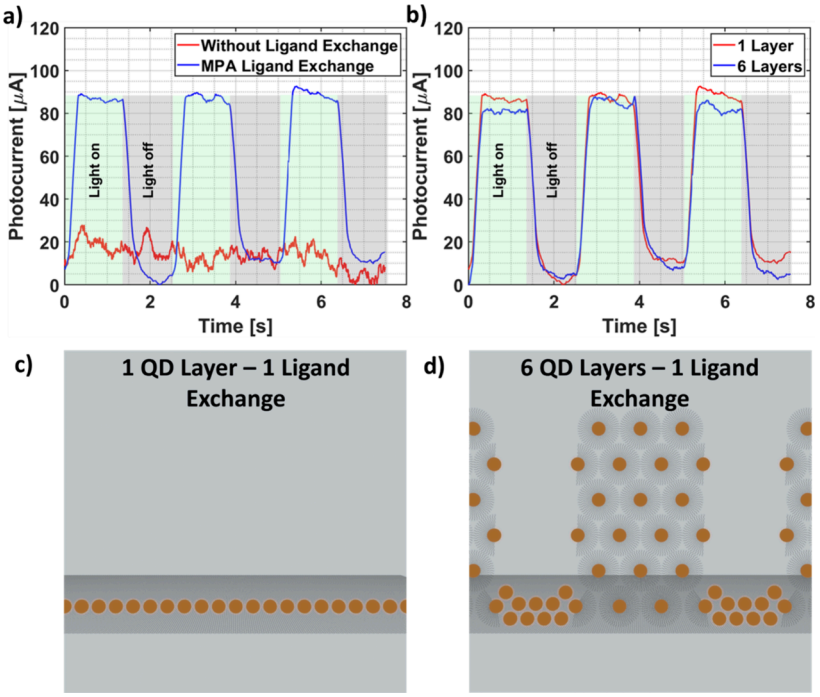


**Figure 3.** (a) Dynamic photoresponse comparison of before and after ligand exchange for a sample with 1 layer of PbS QDs. (b) Comparison of the dynamic photoresponse for 2 different samples, 1 layer and 6 layers of PbS QDs, both with a single MPA ligand exchange. (c,d) Drawings comparing ligand exchange effectiveness for 1 layer and 6 layers, respectively. The need to perform ligand exchange for every layer to ensure all QDs are electrically well connected with MPA can be seen as not all QDs having exchanged OLA/OA with MPA. It should be noted that after the LE, the QD film becomes highly reflective indicating a fairly uniform dispersal of QDs.

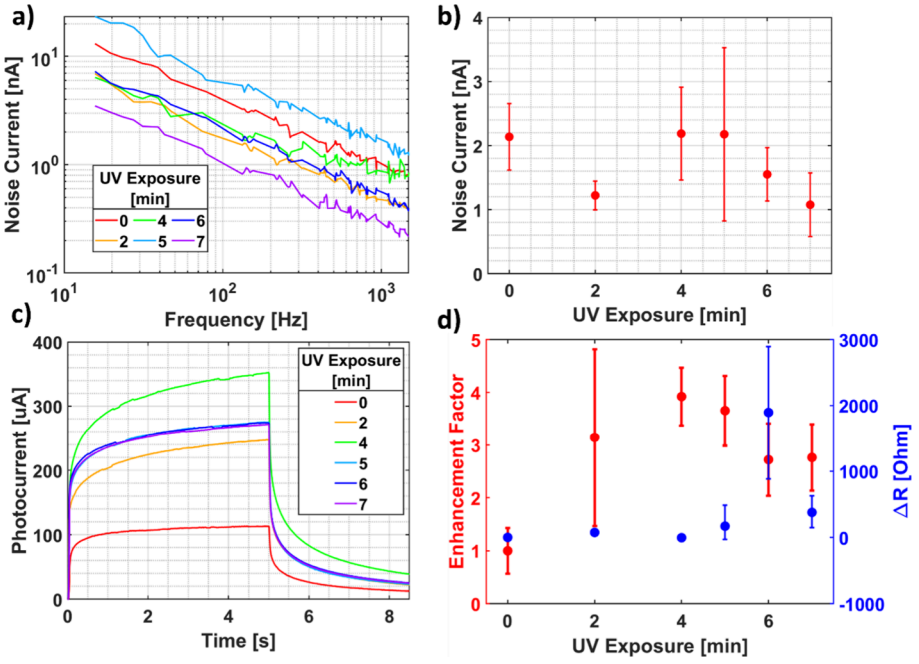


**Figure 4.** (a) Noise spectra for different UVC exposure times. (b) Noise current at a frequency of 60 Hz and 1 V bias voltage for varied UVC exposure times. (c) Dynamic response to 1.5 $\mu$m light. (d) Responsivity enhancement factor for 1.5 $\mu$m light (left-side $y$-axis) and the change in resistance for different UV exposure times (right-side $y$-axis).

Figure 5d from which a decrease in the noise current at low frequencies, by as much as an order of magnitude, after the first QD deposition and ligand exchange can be observed. This is accompanied by an increase in the graphene channel resistance, likely caused by n-type doping of graphene introduced by dangling bonds on the PbS QD surface that were not capped with a MPA ligand or the ligand fell off. While the specific mechanism associated with the noise decrease requires further investigation, we hypothesize that the n-doping of graphene would reduce the p-type doping typical of CVD graphene by adsorbed polar molecules, primarily from air, bringing the Fermi energy closer to the Dirac point or


https://doi.org/10.1021/acsami.4c01115
ACS Appl. Mater. Interfaces 2024, 16, 21302−21310

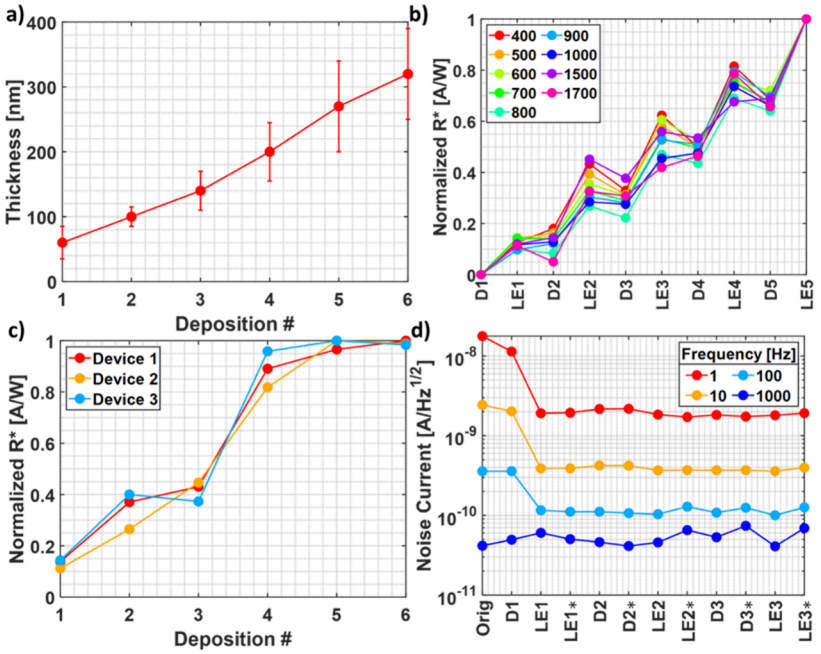


**Figure 5.** (a) PbS QD film thickness vs number of deposition cycles. (b) $R^*$ vs PbS QD depositions (D) and LEs. Note that the $R^*$ values are normalized to that after D5 and LE 5 were completed. (c) Responsivity vs number of depositions, tested under 1500 nm illumination. (d) Noise vs device fabrication step. The steps labeled with an * denote the data was taken with the sample illuminated by a broadband high intensity white light.

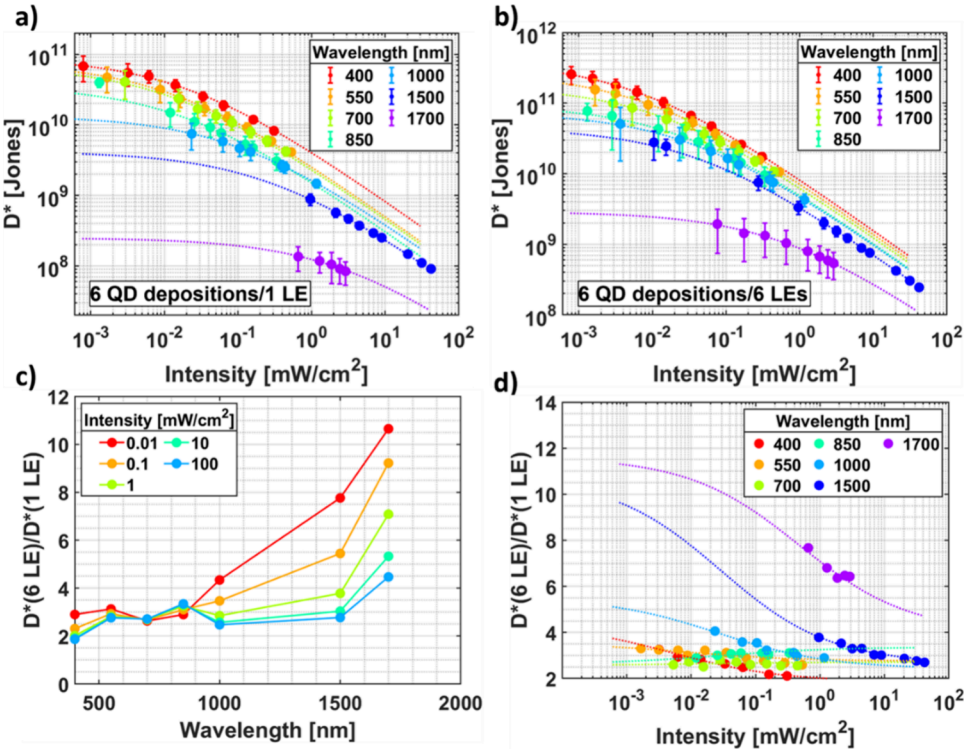


**Figure 6.** (a,b) $D^*$ vs incident light power on the PbS QD/Gr heterostructure devices with 6 depositions and (a) one LE at the end. (b) 6 LEs, one after each deposition, for several wavelengths. (c,d) Predicted $D^*$ enhancement factor between 6 LEs and 1 LE (c) vs wavelength for several incident light powers. (d) vs incident light power for several wavelengths.

closer to the intrinsic charge carrier density and hence lower noise.

$D^*$ can be estimated using the equation of $D^* = \frac{R^*\sqrt{LW\Delta f}}{I_N}$, where $\Delta f$ is the bandwidth, $I_N$ is the noise current, and $L$ and $W$ are the graphene channel length and width, respectively.[44] Figure 6a,b compares the $D^*$ for illumination wavelengths between 400 and 1700 nm and varied light intensity on two samples, both with 6 PbS QD depositions. One sample had only a single ligand exchange at the end of the QD depositions



https://doi.org/10.1021/acsami.4c01115
ACS Appl. Mater. Interfaces 2024, 16, 21302−21310

(Figure 6a) and the other with 6 ligand exchanges, one after each of the 6 QD depositions (Figure 6b). While the two samples show qualitatively similar light intensity dependence at the same wavelengths, the $D^*$ values for the sample with 6 LEs (Figure 6b) are considerably higher by approximately 1 order of magnitude than its counterpart with only 1 LE (Figure 6a). Figure 6c,d displays the enhancement factor between the sample with 6 LEs and that with 1 LE as a function of wavelength and illumination intensity, respectively. The dotted lines in Figure 6d are the predicted enhancement factor from fits to the data points in Figure 6a,b. Interestingly, the enhancement factor increased with the wavelength. In UV−vis spectra, the enhancement factor is in the range of 2−3 while in the SWIR spectrum, it exceeds 10. This indicates that the QD−QD and QD−Gr interfaces would have a more significant impact on optoelectronic performance at longer wavelengths. This is anticipated since a more efficient charge transport is required as the photogenerated changes generated by photons of longer wavelengths would have lower kinetic energies. $D^*$ values of $2.6 \times 10^{11}$, $1.5 \times 10^{11}$, $5 \times 10^{10}$, and $1.9 \times 10^{9}$ Jones at 400, 550, 1000, and 1700 nm were measured for the 6 LE sample that harnessed both QD−QD and QD−Gr interface enhancements. Comparing the 550 nm result ($1.5 \times 10^{11}$ Jones for a light intensity of 1.7 $\mu$W/cm$^2$) to that of Konstantatos et al. (the first report on PbS QD-Gr nanohybrids), the $D^*$ in our work is 2 orders of magnitude lower.[1] The difference can be explained by (1) use of a gate to enhance the charge transfer from QD to graphene, (2) lower light intensity, and (3) smaller QDs, which are optimized for shorter wavelengths with a higher photoconductive gain. We estimate all of these factors would account for at least 2 orders of magnitude (a factor of 2 from (1) and an order of magnitude each from both (2) and (3)), rendering our result comparable with that of Konstantatos et al. Table 1 summarizes recent work on QD/graphene photodetectors.

**Table 1. Summary of Recent Work on QD/Graphene Photodetectors**

| QD material | test wavelength [nm] | $R^*$[A/W] | $D^*$ | ref. |
|---|---|---|---|---|
| PbS | 532 | $10^7$ | $7 \times 10^{13}$ | 1 |
| PbS | 635 | $10^7$ | N/A | 45 |
| PbS | 550 | | $1.5 \times 10^{11}$ | this work |
| $FeS_2$/PbS | 500 | $3.27 \times 10^6$ | $4.89 \times 10^{11}$ | 38 |
| CdS | 450 | 40 | | 46 |
| $Cu_{3-x}P$ | 405 | 9.37 | $5.98 \times 10^{12}$ | 47 |
| $CsPbBr_{3-x}I_x$ | 405 | $8 \times 10^8$ | $2.4 \times 10^{16}$ | 48 |

Lastly, to highlight the importance of balancing light absorption by the QD film and subsequent charge transfer from to graphene, an illustration is presented in Figure 7 of the three possible situations arising from the QD film thickness: too thin, optimal, and too thick. In the case of a QD film that is too thin (Figure 7a), a significant portion of the incident light is not absorbed. The obvious solution would be to increase the film thickness (Figure 7b). Careful attention is required to not overdo the film thickness (Figure 7c) as the likelihood of failed charge dissociation or charge recombination before charge transfer to graphene can occur increases with the thickness of the QD film. While the optimal PbS QD film thickness was found to be around 250 nm, testing is required to define the optimal film thickness for other films of different QD material and/or QD size.

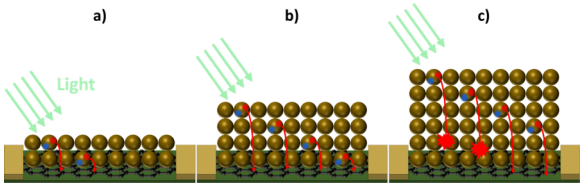


**Figure 7.** Illustration of the balance needed between light absorption and charge transfer to obtain optimal device performance, mediated by the QD film thickness. (a) QD film that is too thin leads to less light absorption, thus less possibility for dissociated exciton charges to be transferred to graphene. (b) Optimum QD film thickness that balances light absorption and charge transfer. (c) QD film that is thicker than optimal absorbs more light but may have charges recombined before transfer to graphene can occur.

## 4. CONCLUSIONS

In summary, this work probed the role of interfaces in PbS QD/Gr nanohybrid photodetectors in terms of the charge transfer across the QD−QD layers and QD/Gr interface during the optoelectronic process for photodetection in a broadband of UV−vis-NIR-SWIR. The critical role of the interfaces on the figures of merit, $R^*$ and $D^*$, has been revealed, and optimization of the charge transfer across QD−QD layers and QD/Gr interface was found imperative to achieving high photodetector performance. In order to obtain efficient photocarrier transfer across the QD−QD interface, a layer-by-layer MPA ligand exchange was developed in this work and a monotonic increase of the $R^*$ with the QD layer coating up to six layers has been observed. In contrast, a single MPA ligand exchange, after completing all six QD layer depositions, yielded a comparable $R^*$ to that of only one QD layer, indicating the majority of photocarriers generated in the six QD coatings were annihilated via recombination with no contribution to $R^*$ due to the lack of efficient charge transfer in the QD layer. To improve the QD/Gr interface for charge transfer from QD to graphene, a UVC irradiation on the graphene was developed to provide cleaning of the graphene surface prior to QD deposition to remove any insulating residues and polar molecules that either block charge transfer or trap transferred charges. Overall, a factor of ∼2−10 and ∼4 improvement in $R^*$ was achieved by layer-by-layer MPA ligand exchange and UVC treatment, respectively. This has yielded high $D^*$ up to $1.5 \times 10^{11}$, $5 \times 10^{10}$, and $1.9 \times 10^{9}$ Jones at 550, 1000, and 1700 nm, respectively.

## ■ ASSOCIATED CONTENT

### Supporting Information

The Supporting Information is available free of charge at https://pubs.acs.org/doi/10.1021/acsami.4c01115.

Source-drain current vs back gate voltage with varied UVC exposure for a graphene field effect transistor; effect on the graphene Raman peak ratios of 2D/G and D/G with varied UVC exposure; PbS QD absorption spectra at various stages in the fabrication process; responsivity stability over the course of 400 days for an array of PbS QD/graphene devices; graphene resistance change over time after UVC exposure of varied duration (PDF)



https://doi.org/10.1021/acsami.4c01115
ACS Appl. Mater. Interfaces 2024, 16, 21302−21310

## AUTHOR INFORMATION


### Corresponding Authors

**Andrew Shultz** − *Department of Physics and Astronomy, The University of Kansas, Lawrence, Kansas 66045, United States;* orcid.org/0009-0007-0106-8903; Email: andjshultz@ku.edu

**Judy Z. Wu** − *Department of Physics and Astronomy, The University of Kansas, Lawrence, Kansas 66045, United States; ZenoLeap LLC, Lawrence, Kansas 66045, United States;* Email: jwu@ku.edu

### Authors

**Bo Liu** − *Department of Physics and Astronomy, The University of Kansas, Lawrence, Kansas 66045, United States;* orcid.org/0000-0003-0298-8238

**Maogang Gong** − *Department of Physics and Astronomy, The University of Kansas, Lawrence, Kansas 66045, United States; ZenoLeap LLC, Lawrence, Kansas 66045, United States;* orcid.org/0000-0002-2031-781X

**Hugo Barragan Vargas** − *Department of Mechanical Engineering Technology, Advanced Manufacturing Institute, University of Houston, Houston, Texas 77204, United States; CIITEC-IPN Cda. de Cecati s/n, CDMX 02250, Mexico*

**Francisco C. Robles Hernandez** − *Department of Mechanical Engineering Technology, Advanced Manufacturing Institute, University of Houston, Houston, Texas 77204, United States; CIITEC-IPN Cda. de Cecati s/n, CDMX 02250, Mexico; Department of Materials Science and NanoEngineering, Rice University, Houston, Texas 77005, United States*

Complete contact information is available at: https://pubs.acs.org/10.1021/acsami.4c01115


### Notes

The authors declare no competing financial interest.

## ACKNOWLEDGMENTS

This research was supported in part by US Army grant W909MY-21-C-0033, and National Science Foundation grants NSF-ECCS-2314401.

## REFERENCES


(1) Konstantatos, G.; Badioli, M.; Gaudreau, L.; Osmond, J.; Bernechea, M.; de Arquer, F. P. G.; Gatti, F.; Koppens, F. H. L. Hybrid Graphene-Quantum Dot Phototransistors with Ultrahigh Gain. *Nat. Nanotechnol.* **2012**, *7* (6), 363−368.

(2) Huang, Y.; Chang, C.; Lin, M.-F. Magnetic and Quantum Confinement Effects on Electronic and Optical Properties of Graphene Ribbons. *Nanotechnology* **2007**, *18* (49), No. 495401.

(3) Dean, C. R.; Young, A. F.; Meric, I.; Lee, C.; Wang, L.; Sorgenfrei, S.; Watanabe, K.; Taniguchi, T.; Kim, P.; Shepard, K. L.; et al. Boron Nitride Substrates for High-Quality Graphene Electronics. *Nat. Nanotechnol.* **2010**, *5* (10), 722−726.

(4) Chen, J. H.; Jang, C.; Xiao, S. D.; Ishigami, M.; Fuhrer, M. S. Intrinsic and Extrinsic Performance Limits of Graphene Devices on Sio2. *Nat. Nanotechnol.* **2008**, *3* (4), 206−209.

(5) Geim, A. K.; Novoselov, K. S. The Rise of Graphene. *Nat. Mater.* **2007**, *6* (3), 183−191.

(6) Geim, A.; Graphene, K. Status and Prospects. *Science* **2009**, *324* (5934), 1530−1534.

(7) Wu, J.; Ma, H.; Yin, P.; Ge, Y.; Zhang, Y.; Li, L.; Zhang, H.; Lin, H. Two-Dimensional Materials for Integrated Photonics: Recent Advances and Future Challenges. *Small Sci.* **2021**, *1* (4), 2000053.

(8) Takagahara, T.; Takeda, K. Theory of the Quantum Confinement Effect on Excitons in Quantum Dots of Indirect-Gap Materials. *Phys. Rev. B* **1992**, *46* (23), 15578.

(9) Guo, R.; Zhang, M.; Ding, J.; Liu, A.; Huang, F.; Sheng, M. Advances in Colloidal Quantum Dot-Based Photodetectors. *J. Mater. Chem. C* **2022**, *10* (19), 7404−7422.

(10) Wu, J.; Chen, S.; Seeds, A.; Liu, H. Quantum Dot Optoelectronic Devices: Lasers, Photodetectors and Solar Cells. *J. Phys. D: Appl. Phys.* **2015**, *48* (36), No. 363001.

(11) Beard, M. C. Multiple Exciton Generation in Semiconductor Quantum Dots. *J. Phys. Chem. Lett.* **2011**, *2* (11), 1282−1288.

(12) Sukhovatkin, V.; Hinds, S.; Brzozowski, L.; Sargent, E. H. Colloidal Quantum-Dot Photodetectors Exploiting Multiexciton Generation. *Science* **2009**, *324* (5934), 1542−1544.

(13) Debellis, D.; Gigli, G.; Ten Brinck, S.; Infante, I.; Giansante, C. Quantum-Confined and Enhanced Optical Absorption of Colloidal Pbs Quantum Dots at Wavelengths with Expected Bulk Behavior. *Nano Lett.* **2017**, *17* (2), 1248−1254.

(14) Lu, H.; Carroll, G. M.; Neale, N. R.; Beard, M. C. Infrared Quantum Dots: Progress, Challenges, and Opportunities. *ACS Nano* **2019**, *13* (2), 939−953.

(15) Koppens, F.; Mueller, T.; Avouris, P.; Ferrari, A.; Vitiello, M.; Polini, M. Photodetectors Based on Graphene, Other Two-Dimensional Materials and Hybrid Systems. *Nat. Nanotechnol.* **2014**, *9* (10), 780−793.

(16) Peng, Z.; Xu, J.; Zhang, J.; Gao, X.; Wang, S. Solution-Processed High-Performance Hybrid Photodetectors Enhanced by Perovskite/Mos2 Bulk Heterojunction. *Adv. Mater. Interfaces* **2018**, *5* (18), 1800505.

(17) Xie, C.; Yan, F. Flexible Photodetectors Based on Novel Functional Materials. *Small* **2017**, *13* (43), 1701822.

(18) Wu, J.; Lu, Y.; Feng, S.; Wu, Z.; Lin, S.; Hao, Z.; Yao, T.; Li, X.; Zhu, H.; Lin, S. The Interaction between Quantum Dots and Graphene: The Applications in Graphene-Based Solar Cells and Photodetectors. *Adv. Funct. Mater.* **2018**, *28* (50), 1804712.

(19) Abid; Sehrawat, P.; Julien, C.; Islam, S. Ws2 Quantum Dots on E-Textile as a Wearable Uv Photodetector: How Well Reduced Graphene Oxide Can Serve as a Carrier Transport Medium? *ACS Appl. Mater. Interfaces* **2020**, *12* (35), 39730−39744.

(20) Dong, C.; Liu, S.; Barange, N.; Lee, J.; Pardue, T.; Yi, X.; Yin, S.; So, F. Long-Wavelength Lead Sulfide Quantum Dots Sensing up to 2600 Nm for Short-Wavelength Infrared Photodetectors. *ACS Appl. Mater. Interfaces* **2019**, *11* (47), 44451−44457.

(21) Shultz, A.; Liu, B.; Gong, M.; Alamri, M.; Walsh, M.; Schmitz, R. C.; Wu, J. Z. Development of Broadband Pbs Quantum Dot/Graphene Photodetector Arrays with High-Speed Readout Circuits for Flexible Imagers. *ACS Appl. Nano Mater.* **2022**, *5* (11), 16896−16905.

(22) Patel, M.; Pataniya, P. M.; Patel, V.; Sumesh, C. Flexible Photodetector Based on Graphite/Zno−Ws2 Nanohybrids on Paper. *Journal of Materials Science: Materials in Electronics* **2022**, *33* (17), 13771−13781.

(23) Ka, I.; Le Borgne, V.; Fujisawa, K.; Hayashi, T.; Kim, Y. A.; Endo, M.; Ma, D.; El Khakani, M. A. Pbs-Quantum-Dots/Double-Wall-Carbon-Nanotubes Nanohybrid Based Photodetectors with Extremely Fast Response and High Responsivity. *Materials Today Energy* **2020**, *16*, No. 100378.

(24) Paul, S.; Ghosh, J.; Hossain, M. T.; Hasebe, H.; Sugimoto, H.; Fujii, M.; Giri, P. K. Interfacial Charge Transfer Induced Enhanced near-Infrared Photoluminescence and Enhanced Visible Photodetection in Two-Dimensional/Zero-Dimensional Bi2se3/Cspbbr2i Heterojunctions with Type-I Band Alignment. *J. Phys. Chem. C* **2022**, *126* (39), 16721−16731.

(25) Pataniya, P. M.; Patel, V.; Sumesh, C. Mos2/Wse2 Nanohybrids for Flexible Paper-Based Photodetectors. *Nanotechnology* **2021**, *32* (31), 315709.

(26) Wu, J.; Gong, M.; Schmitz, R. C.; Liu, B. Quantum Dot/Graphene Heterostructure Nanohybrid Photodetectors. In *Quantum*

*Dot Photodetectors, Lecture Notes in Nanoscale Science and Technology*, Vol. *30*; Springer, Cham, 2021; pp 215−248.
(27) Grotevent, M. J.; Hail, C. U.; Yakunin, S.; Bachmann, D.; Kara, G. k.; Dirin, D. N.; Calame, M.; Poulikakos, D.; Kovalenko, M. V.; Shorubalko, I. Temperature-Dependent Charge Carrier Transfer in Colloidal Quantum Dot/Graphene Infrared Photodetectors. *ACS Appl. Mater. Interfaces* **2021**, *13* (1), 848−856.
(28) Liu, Q.; Gong, Y.; Wilt, J. S.; Sakidja, R.; Wu, J. Synchronous Growth of Ab-Stacked Bilayer Graphene on Cu by Simply Controlling Hydrogen Pressure in Cvd Process. *Carbon* **2015**, *93*, 199.
(29) Xu, G.; Lu, R.; Liu, J.; Chiu, H. Y.; Hui, R.; Wu, J. Z. Photodetection Based on Ionic Liquid Gated Plasmonic Ag Nanoparticle/Graphene Nanohybrid Field Effect Transistors. *Adv. Opt. Mater.* **2014**, *2* (8), 729−736.
(30) Gong, M.; Alamri, M.; Ewing, D.; Sadeghi, S. M.; Wu, J. Z. Localized Surface Plasmon Resonance Enhanced Light Absorption in Aucu/Cspbcl3 Core/Shell Nanocrystals. *Adv. Mater.* **2020**, *32* (26), 2002163.
(31) Cook, B.; Gong, M.; Ewing, D.; Casper, M.; Stramel, A.; Elliot, A.; Wu, J. Inkjet Printing Multicolor Pixelated Quantum Dots on Graphene for Broadband Photodetection. *ACS Appl. Nano Mater.* **2019**, *2* (5), 3246−3252.
(32) Gong, M.; Liu, Q.; Cook, B.; Kattel, B.; Wang, T.; Chan, W. L.; Ewing, D.; Casper, M.; Stramel, A.; Wu, J. Z. All-Printable Zno Quantum Dots/Graphene Van Der Waals Heterostructures for Ultrasensitive Detection of Ultraviolet Light. *ACS Nano* **2017**, *11* (4), 4114−4123.
(33) Kim, S. J.; Han, J.-W.; Kim, B.; Meyyappan, M. Single Walled Carbon Nanotube Based Air Pocket Encapsulated Ultraviolet Sensor. *ACS sensors* **2017**, *2* (11), 1679−1683.
(34) Kang, C. G.; Lee, S. K.; Choe, S.; Lee, Y. G.; Lee, C.-L.; Lee, B. H. Intrinsic Photocurrent Characteristics of Graphene Photodetectors Passivated with Al 2 O 3. *Opt. Express* **2013**, *21* (20), 23391−23400.
(35) Erickson, K.; Erni, R.; Lee, Z.; Alem, N.; Gannett, W.; Zettl, A. Determination of the Local Chemical Structure of Graphene Oxide and Reduced Graphene Oxide. *Adv. Mater.* **2010**, *22* (40), 4467−4472.
(36) Alamri, M. A.; Liu, B.; Walsh, M.; Doolin, J. L.; Berrie, C. L.; Wu, J. Z. Enhanced $H_2$ Sensitivity in Ultraviolet-Activated Pt Nanoparticle/Swcnt/Graphene Nanohybrids. *Ieee Sensors Journal* **2021**, *21* (18), 19762−19770.
(37) Ghopry, S. A.; Liu, B.; Shultz, A.; Wu, J. Z. Tuning Fermi Energy of Graphene Using Platinum Nanoparticles and Ultraviolet Irradiation to Increase Charge Transfer for Surface-Enhanced Raman Spectroscopy. *ACS Appl. Nano Mater.* **2023**, *6* (23), 21626−21633.
(38) Gong, M.; Liu, Q.; Goul, R.; Ewing, D.; Casper, M.; Stramel, A.; Elliot, A.; Wu, J. Z. Printable Nanocomposite Fes2−Pbs Nanocrystals/Graphene Heterojunction Photodetectors for Broadband Photodetection. *ACS Appl. Mater. Interfaces* **2017**, *9* (33), 27801−27808.
(39) Liu, L.; Zhou, H.; Cheng, R.; Yu, W. J.; Liu, Y.; Chen, Y.; Shaw, J.; Zhong, X.; Huang, Y.; Duan, X. High-Yield Chemical Vapor Deposition Growth of High-Quality Large-Area Ab-Stacked Bilayer Graphene. *ACS Nano* **2012**, *6* (9), 8241−8249.
(40) Yan, K.; Peng, H.; Zhou, Y.; Li, H.; Liu, Z. Formation of Bilayer Bernal Graphene: Layer-by-Layer Epitaxy Via Chemical Vapor Deposition. *Nano Lett.* **2011**, *11* (3), 1106−1110.
(41) Zhao, N.; Osedach, T. P.; Chang, L.-Y.; Geyer, S. M.; Wanger, D.; Binda, M. T.; Arango, A. C.; Bawendi, M. G.; Bulovic, V. Colloidal Pbs Quantum Dot Solar Cells with High Fill Factor. *ACS Nano* **2010**, *4* (7), 3743−3752.
(42) Becker-Koch, D.; Albaladejo-Siguan, M.; Lami, V.; Paulus, F.; Xiang, H.; Chen, Z.; Vaynzof, Y. Ligand Dependent Oxidation Dictates the Performance Evolution of High Efficiency Pbs Quantum Dot Solar Cells. *Sustainable Energy & Fuels* **2020**, *4* (1), 108−115.
(43) Georgitzikis, E.; Malinowski, P. E.; Maes, J.; Hadipour, A.; Hens, Z.; Heremans, P.; Cheyns, D. Optimization of Charge Carrier Extraction in Colloidal Quantum Dots Short-Wave Infrared Photodiodes through Optical Engineering. *Adv. Funct. Mater.* **2018**, *28* (42), 1804502.
(44) Jones, R. C. Proposal of the Detectivity D** for Detectors Limited by Radiation Noise. *JOSA* **1960**, *50* (11), 1058−1059.
(45) Ahn, S.; Chung, H.; Chen, W.; Moreno-Gonzalez, M. A.; Vazquez-Mena, O. Optoelectronic Response of Hybrid Pbs-Qd/Graphene Photodetectors. *J. Chem. Phys.* **2019**, *151* (23), 234705 DOI: 10.1063/1.5132562.
(46) Chan, Y.; Dahua, Z.; Jun, Y.; Linlong, T.; Chongqian, L.; Jun, S. Fabrication of Hybrid Graphene/Cds Quantum Dots Film with the Flexible Photo-Detecting Performance. *Physica E: Low-dimensional Systems and Nanostructures* **2020**, *124*, No. 114216.
(47) Sun, T.; Wang, Y.; Yu, W.; Wang, Y.; Dai, Z.; Liu, Z.; Shivananju, B. N.; Zhang, Y.; Fu, K.; Shabbir, B.; Ma, W.; Li, S.; Bao, Q. Flexible Broadband Graphene Photodetectors Enhanced by Plasmonic Cu3− Xp Colloidal Nanocrystals. *Small* **2017**, *13* (42), 1701881.
(48) Kwak, D.-H.; Lim, D.-H.; Ra, H.-S.; Ramasamy, P.; Lee, J.-S. High Performance Hybrid Graphene−Cspbbr 3− X I X Perovskite Nanocrystal Photodetector. *RSC Adv.* **2016**, *6* (69), 65252−65256.